Single-photon emission and scattering in quadratically-coupled optomechanical models

Jie-Qiao Liao[1] and Franco Nori[1, 2, 3]

[1]*CEMS, RIKEN, Saitama 351-0198, Japan*
[2]*Department of Physics, The University of Michigan, Ann Arbor, Michigan 48109-1040, USA*
[3]*Department of Physics, Korea University, Seoul 136-713, Korea*

(Dated: May 2, 2013)

We present exact analytical solutions to study the coherent interaction between a single photon and the mechanical motion of a membrane in *quadratically*-coupled optomechanics. We consider single-photon emission when the photon is initially inside the cavity. We also consider single-photon scattering when the photon wavepacket is initially in the fields outside the cavity. Using our solutions, we calculate the single-photon emission and scattering spectra, and build the connection between the spectral features and the system's inherent parameters, such as: the coupling strength, the mechanical frequency, and the cavity decay rate. In particular, we clarify the conditions for the phonon sidebands to be visible.

PACS numbers: 42.50.Pq, 42.50.Wk, 07.10.Cm

I. INTRODUCTION

The coherent coupling between electromagnetic and mechanical degrees of freedom via radiation pressure is at the heart of cavity optomechanics [1–3]. In general, optomechanical couplings can be classified into two categories: linear or quadratic couplings. Namely, the coupling term is proportional to either x or x^2 (x being the mechanical displacement). For a mechanical resonator, the linear coupling leads to the displacement of its equilibrium position, while the quadratic coupling changes its resonant frequency.

To understand and exploit the optomechanical couplings, it is highly desirable to realize the couplings in the single-photon strong-coupling regime, in which the couplings involving a single photon can produce observable effects on both mechanical and electromagnetic signals. Such a regime is important to test the fundamentals of quantum theory [4–7] and to explore possible applications of optomechanical devices to future quantum technology [8, 9]. In the past several years, considerable advances have been made in the single-photon strong-coupling regime of linear coupling [10–21]. However, for the quadratic coupling, though much attention has been paid to this area [22–39], not much work has been devoted to the single-photon strong-coupling regime because the attainable coupling strength is weak. Interestingly, recent experiments indicate that the quadratic coupling strength can be increased significantly using a fiber cavity with a smaller mode size, and a smaller and lighter membrane [34]. Motivated by this, it is of interest to study the quadratic optomechanical coupling in the single-photon strong-coupling regime.

When a quadratically-coupled optomechanical cavity works in the single-photon strong-coupling regime, the frequency change of the mechanical resonator induced by a single photon will significantly affect the cavity field, causing some observable features in the cavity photon spectrum. Thus, a natural question is how the spectrum may characterize the single-photon strong-coupling regime. In this paper, we answer this question by calculating analytically the spectrum of single-photon emission and scattering. In particular, we build a connection between the spectral features and the system's inherent parameters, such as: the coupling strength, the membrane's resonant frequency, and the cavity decay rate. We also clarify the condition for observing the phonon sidebands in the spectra.

II. THE MODEL

To be specific, we consider a quadratically-coupled optomechanical system with a "membrane-in-the-middle" configuration [see Fig. 1(a)], where a thin dielectric membrane is placed inside a Fabry-Pérot cavity. We model the moving membrane as a harmonic oscillator and focus on a single-mode field in the cavity. When the membrane is placed at a node (or antinode) of the intracavity standing wave, the cavity field will quadratically couple to the mechanical motion of the membrane. The Hamiltonian (with $\hbar = 1$) of the quadratically-coupled optomechanical cavity is [22]

$$H_{\rm opc} = \omega_c a^\dagger a + \omega_M b^\dagger b + g a^\dagger a (b^\dagger + b)^2, \tag{1}$$

where a ($a^\dagger$) and b ($b^\dagger$) are, respectively, the annihilation (creation) operators of the single-mode cavity field and the mechanical motion of the membrane, with the respective resonant frequencies ω_c and ω_M. The third term in Eq. (1) describes a quadratic optomechanical coupling with a strength g between the cavity field and the membrane. To keep the stability of the membrane, the strength g should satisfy the condition $(\omega_M + 4mg) > 0$, where m is the number of the photons inside the cavity.

The photon number operator $a^\dagger a$ in Hamiltonian $H_{\rm opc}$ is a conserved quantity, and hence for a given photon number m, the coupling actually takes a quadratic form $mg(b^\dagger+b)^2$, which can be diagonalized with the single-mode squeezing transformation. Denoting the harmonic-oscillator number states of the cavity and the membrane as $|m\rangle_a$ and $|n\rangle_b$ $(m, n = 0, 1, 2, ...)$ respectively, then the eigensystem of the Hamiltonian $H_{\rm opc}$ can be obtained as

$$H_{\rm opc}|m\rangle_a|\tilde{n}(m)\rangle_b = (m\omega_c + n\omega_M^{(m)} + \delta^{(m)})|m\rangle_a|\tilde{n}(m)\rangle_b, \tag{2}$$

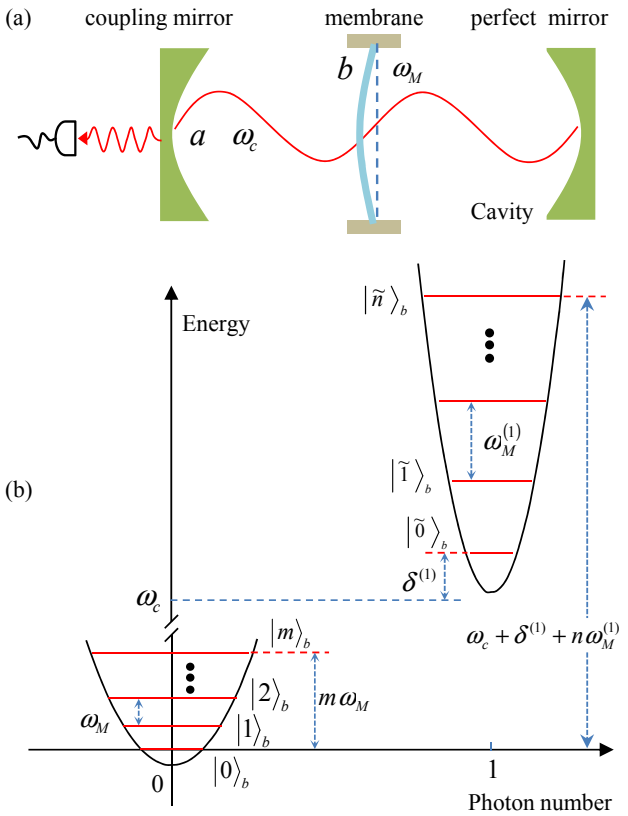

FIG. 1. (Color online) (a) Schematic diagram of a quadratically-coupled optomechanical system with a "membrane-in-the-middle" configuration. (b) The diagram of the energy-level structure (unscaled) of the optomechanical system when the cavity is in a vacuum or contains a single photon.

where we introduce the m-photon coupled membrane's resonant frequency $\omega_M^{(m)}$ and frequency shift $\delta^{(m)}$,

$$\omega_M^{(m)} = \omega_M\sqrt{1+\frac{4mg}{\omega_M}}, \tag{3a}$$

$$\delta^{(m)} = \frac{1}{2}(\omega_M^{(m)}-\omega_M). \tag{3b}$$

The m-photon squeezed number state in Eq. (2) is defined by

$$|\tilde{n}(m)\rangle_b = S_b(\eta_m)|n\rangle_b, \tag{4}$$

where $S_b(\eta_m)=\exp[\frac{\eta_m}{2}(b^2-b^{\dagger 2})]$ is a squeezing operator with the squeezing factor

$$\eta_m = \frac{1}{4}\ln\left(1+\frac{4mg}{\omega_M}\right). \tag{5}$$

We note that the eigensystem of the Hamiltonian (1) has been derived in previous studies [25, 37]. In the zero-photon case, we have $|\tilde{n}(0)\rangle_b = |n\rangle_b$, $\omega_M^{(0)}=\omega_M$, and $\delta^{(0)}=0$. For convenience, the energy-level structure of the system in the zero- and one-photon cases is shown in Fig. 1(b).

To include the dissipation of the cavity field, we assume that the cavity photons can couple with the outside fields through the coupling mirror. Without loss of generality, we model the environment of the cavity as a harmonic-oscillator bath. Then the Hamiltonian of the whole system including the optomechanical cavity and the environment can be written as

$$H = H_{\rm opc} + \int_0^\infty \omega_k c_k^\dagger c_k dk + \xi\int_0^\infty (ac_k^\dagger + c_k a^\dagger)dk, \tag{6}$$

where the annihilation operator c_k describes the kth mode of the outside fields with resonant frequency ω_k. The coupling between the cavity field and the outside fields is described by the hopping interaction with strength ξ. Since the decay rate γ_m of the mechanical resonator is much smaller than the decay rate γ_c of the cavity, then during the emission and scattering time interval $1/\gamma_c \ll t \ll 1/\gamma_m$, the damping of the membrane is negligible. In this work we take into account the dissipation of the cavity and neglect the mechanical dissipation.

In the rotating frame with respect to $H_0 = \omega_c a^\dagger a + \omega_c\int_0^\infty c_k^\dagger c_k dk$, the Hamiltonian (6) becomes

$$H_I = \omega_M b^\dagger b + g a^\dagger a(b^\dagger+b)^2 + \int_0^\infty \Delta_k c_k^\dagger c_k dk + \xi\int_0^\infty (ac_k^\dagger + c_k a^\dagger)dk, \tag{7}$$

where $\Delta_k = \omega_k - \omega_c$ is the detuning of the kth mode photon from the cavity frequency. The total photon number, $N = a^\dagger a + \int_0^\infty c_k^\dagger c_k dk$, in the whole system is a conserved quantity because of $[N, H_I]=0$. Denoting $|\tilde{m}(1)\rangle_b = |\tilde{m}\rangle_b$ for conciseness, a general state in the single-photon subspace of the total system can be written as

$$|\varphi(t)\rangle = \sum_{m=0}^\infty A_m(t)|1\rangle_a|\tilde{m}\rangle_b|\emptyset\rangle + \sum_{m=0}^\infty\int_0^\infty B_{m,k}(t)|0\rangle_a|m\rangle_b|1_k\rangle dk, \tag{8}$$

where $|1\rangle_a|\tilde{m}\rangle_b|\emptyset\rangle$ denotes the state with the cavity in the single-photon state $|1\rangle_a$, the membrane in the single-photon squeezed number state $|\tilde{m}\rangle_b$ (hereafter we call it as squeezed number state for conciseness), and the outside fields in a vacuum $|\emptyset\rangle$. Also $|0\rangle_a|m\rangle_b|1_k\rangle$ denotes the state with a vacuum cavity field $|0\rangle_a$, the membrane in the number state $|m\rangle_b$, and one photon in the kth mode of the outside fields $|1_k\rangle$.

We point out that these squeezed number states in Eq. (8) satisfy the completeness $\sum_{m=0}^\infty |\tilde{m}\rangle_b\langle\tilde{m}|_b = I_b$ (I_b is the identity operator in the Hilbert space of mode b) and orthogonality $\langle\tilde{m}|_b|\tilde{n}\rangle_b = \delta_{m,n}$. Moreover, the overlap $\langle m|_b|\tilde{n}\rangle_b = \langle m|_b S_b(\eta_1)|n\rangle_b$ between the squeezed number state $|\tilde{n}\rangle_b$ and the harmonic-oscillator number state $|m\rangle_b$ is determined by the relation

$$\langle m|_b S_b(\eta_1)|n\rangle_b = \frac{\sqrt{m!n!}}{(\cosh\eta_1)^{n+1/2}}\sum_{l'=0}^{\mathrm{Floor}[\frac{m}{2}]}\sum_{l=0}^{\mathrm{Floor}[\frac{n}{2}]}\frac{(-1)^{l'}}{l!l'!}\times\frac{(\frac{1}{2}\tanh\eta_1)^{l+l'}}{(n-2l)!}(\cosh\eta_1)^{2l}\delta_{m-2l',n-2l}, \tag{9}$$

where $\eta_1 = (1/4)\ln(1+4g/\omega_M)$ and the function Floor$[x]$ gives the greatest integer less than or equal to x.

According to Eqs. (7), (8), and the Schrödinger equation $i\frac{\partial}{\partial t}|\varphi(t)\rangle = H_I|\varphi(t)\rangle$, we obtain the equations of motion for the probability amplitudes

$$\dot{A}_m(t) = -i(\delta^{(1)} + m\omega_M^{(1)})A_m(t) - i\xi\sum_{n=0}^{\infty}\int_0^{\infty}\langle\tilde{m}|_b|n\rangle_b B_{n,k}(t)dk, \quad (10a)$$

$$\dot{B}_{m,k}(t) = -i(\Delta_k + m\omega_M)B_{m,k}(t) - i\xi\sum_{n=0}^{\infty}\langle m|_b|\tilde{n}\rangle_b A_n(t), \quad (10b)$$

where the single-photon coupled membrane's frequency and frequency shift are given by $\omega_M^{(1)} = \omega_M\sqrt{1+4g/\omega_M}$ and $\delta^{(1)} = (\omega_M^{(1)} - \omega_M)/2$. In addition, the coefficients $\langle\tilde{m}|_b|n\rangle_b$ and $\langle m|_b|\tilde{n}\rangle_b$ can be calculated using Eq. (9). In principle, the state of the whole system can be obtained by solving the equations of motion (10) under a given initial condition. In the following, we will consider single-photon emission and scattering.

III. SINGLE-PHOTON EMISSION

In the emission case, a single photon is initially inside the cavity, and the outside fields are in a vacuum. Without loss of generality, we assume that the initial state of the membrane is an arbitrary number state $|n_0\rangle_b$. Once the solution in this case is obtained, the solution for the general initial membrane state can be obtained accordingly by superposition. For the initial state $|1\rangle_a|n_0\rangle_b|\emptyset\rangle$, the corresponding initial condition for Eq. (10) reads $A_m(0) = \langle\tilde{m}|_b|n_0\rangle_b$ and $B_{m,k}(0) = 0$. For the purpose of studying single-photon emission, we will focus on the long-time state of the system. The long-time solution for these probability amplitudes is $A_{n_0,m}(\infty) = 0$ and

$$B_{n_0,m,k}(\infty) = \sum_{n=0}^{\infty}\frac{\sqrt{\gamma_c/2\pi}\langle m|_b|\tilde{n}\rangle_b\langle\tilde{n}|_b|n_0\rangle_b e^{-i(\Delta_k+m\omega_M)t}}{\Delta_k - \delta^{(1)} - n\omega_M^{(1)} + m\omega_M + i\frac{\gamma_c}{2}}, \quad (11)$$

where $\gamma_c = 2\pi\xi^2$ is the cavity decay rate, and we add the subscript n_0 in $A_{n_0,m}(t)$ and $B_{n_0,m,k}(t)$ to mark the membrane's initial state $|n_0\rangle_b$.

In the long-time limit, the single photon completely leaks out of the cavity and hence the cavity is in a vacuum $[A_{n_0,m}(\infty) = 0]$. The amplitude $B_{n_0,m,k}(\infty)$ exhibits a clear physical picture for the single-photon emission. Specifically, the initial state $|1\rangle_a|n_0\rangle_b$ can be expanded as $\sum_{n=0}^{\infty} c_{n_0,n}|1\rangle_a|\tilde{n}\rangle_b$, with $c_{n_0,n} = \langle\tilde{n}|_b|n_0\rangle_b$. For each component $|1\rangle_a|\tilde{n}\rangle_b$, the single-photon emission process induces the transition $|1\rangle_a|\tilde{n}\rangle_b \to |0\rangle_a|m\rangle_b$. The corresponding transition amplitude is proportional to the numerator in Eq. (11). Due to the quadratic terms of b and $b^\dagger$ in $S_b(\eta_1)$, $|m\rangle_b$ and $|\tilde{n}\rangle_b$ should have the same parity, i.e., being odd or even. Consequently, the phonon number distribution in the long-time state of the membrane will have the same parity as its initial component $|n_0\rangle_b$. In addition, we can derive the resonant condition in this emission process from the energy-level structure in Fig. 1(b). For the transition $|1\rangle_a|\tilde{n}\rangle_b \to |0\rangle_a|m\rangle_b$, the frequency of the emitted photon is $\omega_k = \omega_c + \delta^{(1)} + n\omega_M^{(1)} - m\omega_M$, which is consistent with the resonance condition

$$\Delta_k = \delta^{(1)} + n\omega_M^{(1)} - m\omega_M, \quad (12)$$

obtained from the pole of the denominator in Eq. (11).

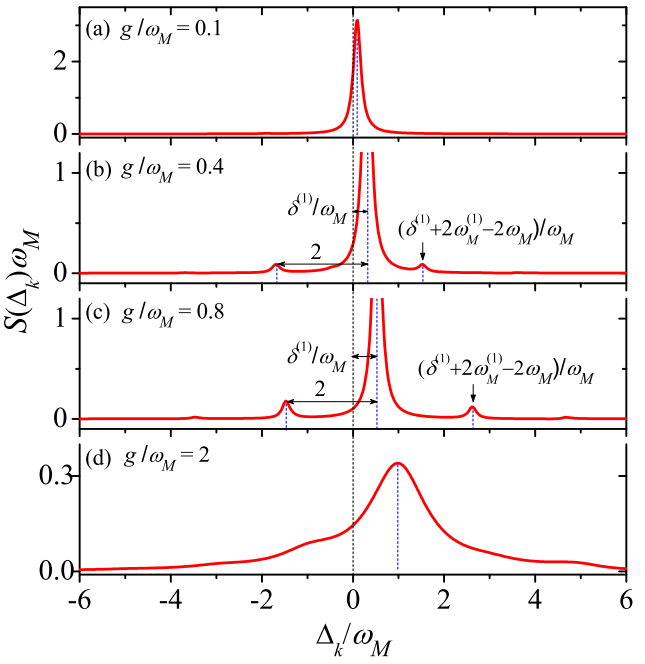

FIG. 2. (Color online) Single-photon emission spectrum $S(\Delta_k)$ as a function of Δ_k for various values of g and γ_c. Panels (a-c) are plotted in the resolved-sideband regime ($\gamma_c/\omega_M = 0.2$), while (d) is plotted in the unresolved-sideband regime ($\gamma_c/\omega_M = 1.5$). The membrane's initial state is $|0\rangle_b$.

We know from Eqs. (8) and (11) that, corresponding to the initial state $|1\rangle_a|n_0\rangle_b|\emptyset\rangle$, the long-time state of the whole system is

$$|\varphi_{n_0}(\infty)\rangle = \sum_{m=0}^{\infty}\int_0^{\infty} B_{n_0,m,k}(\infty)|0\rangle_a|m\rangle_b|1_k\rangle dk. \quad (13)$$

Therefore, when the membrane is initially in a general density matrix

$$\rho^{(b)}(0) = \sum_{m,n=0}^{\infty}\rho_{m,n}^{(b)}(0)|m\rangle_b\langle n|_b, \quad (14)$$

the long-time state of the whole system can be obtained by superposition as

$$\rho(\infty) = \sum_{m,n=0}^{\infty}\rho_{m,n}^{(b)}(0)|\varphi_m(\infty)\rangle\langle\varphi_n(\infty)|. \quad (15)$$

Here the density matrix elements are $\rho_{m,n}^{(b)}(0) = \langle m|_b\rho^{(b)}(0)|n\rangle_b$. For a pure state $|\phi(0)\rangle_b = \sum_{n=0}^{\infty} c_n|n\rangle_b$ and a mixed state $\rho^{(b)}(0) = \sum_{n=0}^{\infty} p_n|n\rangle_b\langle n|_b$, the matrix elements are $\rho_{m,n}^{(b)}(0) = c_m c_n^*$ and $\rho_{m,n}^{(b)}(0) = p_n\delta_{m,n}$, respectively.

To characterize the quadratic optomechanical coupling, a useful quantity is the single-photon emission spectrum, i.e., the probability distribution of the emitted photon. For the initial membrane state (14), the emission spectrum is defined by

$$S(\Delta_k) = \mathrm{Tr}[|1_k\rangle\langle 1_k|\rho(\infty)] = \sum_{l,m,n=0}^{\infty} \rho^{(b)}_{m,n}(0) B_{m,l,k}(\infty) B^{*}_{n,l,k}(\infty). \quad (16)$$

In Fig. 2, we plot the emission spectrum $S(\Delta_k)$ versus the photon frequency Δ_k, for various values of g and γ_c, when the membrane is initially in its ground state $|0\rangle_b$. Figures 2(a-c) are plotted in the resolved-sideband regime $\omega_M > \gamma_c$ [40] so that the phonon sideband peaks could be used to characterize the coupling strength g. When $g < \gamma_c$ [Fig. 2(a)], the spectrum is approximately a Lorentzian function with width γ_c and center $\Delta_k = \delta^{(1)}$. In this case, there are no sideband peaks in the spectrum. However, the sideband peaks become visible when $g > \gamma_c$. Physically, when the displacement of the membrane equals its zero-point fluctuation, the photon frequency shift induced by the quadratic optomechanical coupling is g. To resolve this frequency shift from the Lorentzian spectrum of a free cavity, the condition $g > \gamma_c$ should be satisfied. Such a condition can also be understood by examining the height of these peaks in the spectrum. To resolve a peak in the spectrum, the peak height should be much higher than the tail of its neighboring Lorentzian. This requires $g \gg \gamma_c$ in the resolved-sideband regime. As an example, we analyze the special case of $g/\omega_M \ll 1$. In the resolved-sideband regime $\omega_M/\gamma_c \gg 1$ and under the initial state $|0\rangle_b$, we expand $S(\Delta_k)$ up to second-order in g/ω_M. Then, the height of the sideband peak located at $\Delta_k = \delta^{(1)} - 2\omega_M$ can be obtained as $S(\delta^{(1)} - 2\omega_M) \approx (\gamma_c/8\pi\omega_M^2)(1 + 8g^2/\gamma_c^2)$. Since the main peak of the spectrum is approximately a Lorentzian function $S_L(\Delta_k) \approx \frac{\gamma_c}{2\pi}[(\Delta_k - \delta^{(1)})^2 + \gamma_c^2/4]^{-1}$, then the requirement

$$\frac{S(\delta^{(1)} - 2\omega_M)}{S_L(\delta^{(1)} - 2\omega_M)} \approx 1 + \frac{8g^2}{\gamma_c^2} \gg 1 \quad (17)$$

leads to the condition $g \gg \gamma_c$.

We remark that the positions of these sideband peaks in Fig. 2 are determined by the resonance condition (12), and these sideband peaks are not periodic because of the difference between $\omega_M^{(1)}$ and ω_M. Also, for the initial state $|0\rangle_b$ of the membrane, the contributing m and n in Eq. (12) should be even numbers due to the parity requirement. In Figs. 2(a-c), the peak located at $\Delta_k = \delta^{(1)}$ is the main peak (corresponding to the transition $|1\rangle_a|\tilde{0}\rangle_b \rightarrow |0\rangle_a|0\rangle_b$). Hence, we can resolve the main peak from the Lorentzian spectrum for a free cavity when $\delta^{(1)} > \gamma_c$, which requires $g > \gamma_c(1 + \gamma_c/\omega_M)$. The peak located at $\Delta_k = \delta^{(1)} - 2\omega_M$ corresponds to the transition $|1\rangle_a|\tilde{0}\rangle_b \rightarrow |0\rangle_a|2\rangle_b$. Moreover, the peak located at $\Delta_k = \delta^{(1)} + 2\omega_M^{(1)} - 2\omega_M$ corresponds to the transition $|1\rangle_a|\tilde{2}\rangle_b \rightarrow |0\rangle_a|2\rangle_b$. Finally, Fig. 2(d) is plotted in the unresolved-sideband regime. We can see from Fig. 2(d) that, though the system works in the single-photon strong-coupling regime, there are no sideband peaks in the spectrum. This fact indicates that the resolved-sideband regime and the single-photon strong-coupling condition are two necessary requirements for observing sideband peaks in the emission spectrum.

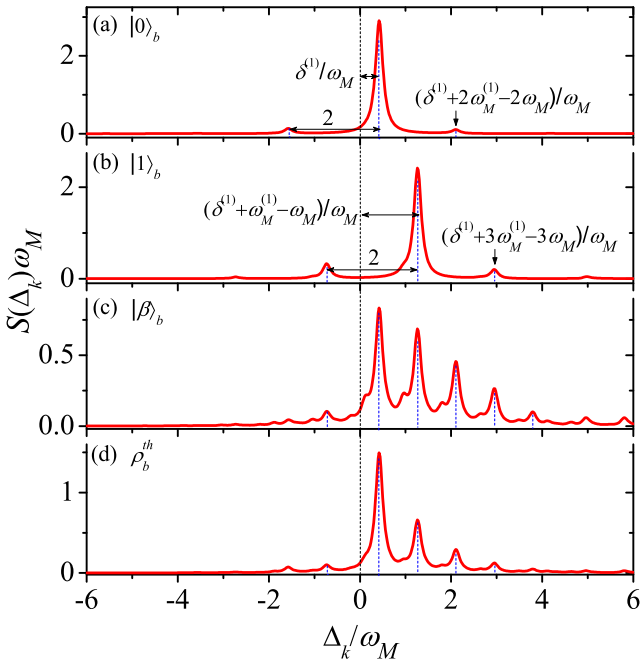

FIG. 3. (Color online) Single-photon emission spectrum $S(\Delta_k)$ as a function of Δ_k when the initial state of the membrane is either the Fock states $|0\rangle_b$ and $|1\rangle_b$, the coherent state $|\beta = 1\rangle_b$, or the thermal state $\rho_b^{th}(\bar{n} = 1)$. Other parameters are $\gamma_c/\omega_M = 0.2$ and $g/\omega_M = 0.6$.

To illustrate how the spectrum depends on the initial state of the membrane, we plot in Fig. 3 the spectrum $S(\Delta_k)$ versus Δ_k when the membrane is initially in either the Fock states $|0\rangle_b$ and $|1\rangle_b$, the coherent state $|\beta = 1\rangle_b$, or the thermal state $\rho_b^{th}(\bar{n} = 1)$. For the initial state $|0\rangle_b$, the main peak (with the location $\Delta_k = \delta^{(1)}$) in Fig. 3(a) is related to the transition $|1\rangle_a|\tilde{0}\rangle_b \rightarrow |0\rangle_a|0\rangle_b$. The two peaks located at $\Delta_k = \delta^{(1)} - 2\omega_M$ and $\Delta_k = \delta^{(1)} + 2\omega_M^{(1)} - 2\omega_M$ correspond to the transitions $|1\rangle_a|\tilde{0}\rangle_b \rightarrow |0\rangle_a|2\rangle_b$ and $|1\rangle_a|\tilde{2}\rangle_b \rightarrow |0\rangle_a|2\rangle_b$, respectively. For the initial state $|1\rangle_b$, the main peak (located at $\Delta_k = \delta^{(1)} + \omega_M^{(1)} - \omega_M$) in Fig. 3(b) is related to the transition $|1\rangle_a|\tilde{1}\rangle_b \rightarrow |0\rangle_a|1\rangle_b$. The other two peaks located at $\Delta_k = \delta^{(1)} + \omega_M^{(1)} - 3\omega_M$ and $\Delta_k = \delta^{(1)} + 3\omega_M^{(1)} - 3\omega_M$ correspond to the transitions $|1\rangle_a|\tilde{1}\rangle_b \rightarrow |0\rangle_a|3\rangle_b$ and $|1\rangle_a|\tilde{3}\rangle_b \rightarrow |0\rangle_a|3\rangle_b$, respectively. Here, Figs. 3(a) and (b) only show even- and odd-parity sideband peaks, respectively. However, the coherent and thermal states contain both odd- and even-parity number states, and hence we can see both odd- and even-parity sideband peaks in Figs. 3(c,d). The positions of these sideband peaks are consistent with those in Figs. 3(a,b).

IV. SINGLE-PHOTON SCATTERING

We now turn to the single-photon scattering case. In this case, the single photon is initially in a Lorentzian wave packet in the outside fields, and the cavity is in a vacuum $|0\rangle_a$. We

also assume that the membrane is initially in the number state $|n_0\rangle_b$, and then the initial condition for Eq. (10) becomes

$$A_m(0) = 0, \qquad B_{m,k}(0) = \sqrt{\frac{\epsilon}{\pi}}\frac{1}{\Delta_k - \Delta_0 + i\epsilon}\delta_{m,n_0}, \quad (18)$$

where Δ_0 and ϵ are the detuning center and spectral width of the photon, respectively. Based on this initial condition (18) and Eq. (10), the long-time solution ($t \gg 1/\gamma_c, 1/\epsilon$) of these probability amplitudes is $A_{n_0,m}(\infty) = 0$ and

$$\begin{aligned} B_{n_0,m,k}(\infty) = e^{-i(\Delta_k + m\omega_M)t}\Bigg(& \sqrt{\frac{\epsilon}{\pi}}\frac{1}{\Delta_k - \Delta_0 + i\epsilon}\delta_{m,n_0} \\ & - \sqrt{\frac{\epsilon}{\pi}}\frac{1}{\Delta_k - [\Delta_0 + (n_0 - m)\omega_M] + i\epsilon} \\ & \times \sum_{n=0}^{\infty}\frac{i\gamma_c \langle m|_b|\tilde{n}\rangle_b\langle\tilde{n}|_b|n_0\rangle_b}{\Delta_k - \delta^{(1)} - n\omega_M^{(1)} + m\omega_M + i\frac{\gamma_c}{2}}\Bigg). \end{aligned} \quad (19)$$

In the long-time limit, the single photon will completely leak out of the cavity, and hence we have $A_{n_0,m}(\infty) = 0$. It can be seen from $B_{n_0,m,k}(\infty)$ that there are two physical processes in the single-photon scattering. (i) The single-photon direct-reflection process: the incident photon is directly reflected by the mirror, without entering the cavity. This process is described by the first term of $B_{n_0,m,k}(\infty)$. (ii) The photon-membrane interacting process: the single photon enters the cavity to couple with the moving membrane and eventually leaks out of the cavity via the cavity decay channel. This process is described by the second term (i.e., the second and third line) in Eq. (19). In this process, the system experiences the transitions $|0\rangle_a|n_0\rangle_b \to |1\rangle_a|\tilde{n}\rangle_b \to |0\rangle_a|m\rangle_b$, These transitions are governed by the two resonance conditions

$$\Delta_0 = \delta^{(1)} + n\omega_M^{(1)} - n_0\omega_M, \quad (20a)$$

$$\Delta_k = \delta^{(1)} + n\omega_M^{(1)} - m\omega_M, \quad (20b)$$

which can be derived from either the energy level structure in Fig. 1(b) or the poles of the probability amplitude (19). Interestingly, the second line in Eq. (19) is a Lorentzian wave packet with spectral width ϵ and center $\Delta_k = \Delta_0 + (n_0 - m)\omega_M$. In comparison to the initial Lorentzian wave packet (18), the shift of the wave packet center is equal to the energy variance of the membrane. Moreover, the third line in Eq. (19) has a similar form as Eq. (11) for the single-photon emission process.

The single-photon scattering spectrum can be calculated in terms of Eqs. (16) and (19). We see from Eq. (19) that either the second line or the third line could cause phonon sidebands, and the conditions for resolving these sidebands due to the two lines are $\omega_M > \epsilon$ and $\omega_M > \gamma_c$, respectively. Here, γ_c is the system's inherent parameter while ϵ is an externally controllable parameter. In the following, we first consider the case of $\epsilon > \omega_M > \gamma_c$ so that the observed sideband peaks are caused purely by the system inherent effect. In Fig. 4, we plot the spectrum $S(\Delta_k)$ versus the photon frequency Δ_k for various values of g and γ_c. When $g < \gamma_c$, there are no peaks in the spectrum [Fig. 4(a)]. The phonon sideband effect can be observed in the scattering spectrum when $g > \gamma_c$

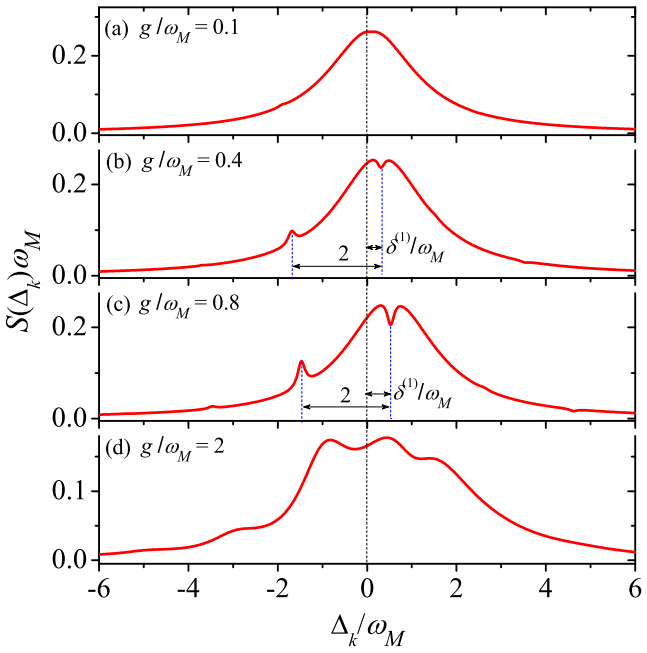

FIG. 4. (Color online) Single-photon scattering spectrum $S(\Delta_k)$ versus the photon frequency Δ_k for various values of g and γ_c. Figures (a-c) are plotted in the resolved-sideband regime ($\gamma_c/\omega_M = 0.2$), while (d) is plotted in the unresolved-sideband regime ($\gamma_c/\omega_M = 1.5$). The membrane's initial state is $|0\rangle_b$. Other parameter are $\Delta_0 = \delta^{(1)}$ and $\epsilon/\omega_M = 1.2$.

and $\omega_M > \gamma_c$ [Figs. 4(b,c)]. Owing to the interference between the direct reflection process and the photon-membrane interacting process, there exist both peaks and dips in the spectrum. In Figs. 4(b,c), the dips represent the transition $|1\rangle_a|\tilde{0}\rangle_b \to |0\rangle_a|0\rangle_b$, while the peaks correspond to the transition $|1\rangle_a|\tilde{0}\rangle_b \to |0\rangle_a|2\rangle_b$. In addition, in the unresolved-sideband regime ($\gamma_c > \omega_M$), there are no peaks even in the single-photon strong-coupling regime [Fig. 4(d)].

We now consider the near-monochromatic case ($\epsilon \ll \gamma_c$). In Fig. 5(a), we plot the scattering spectrum in the case of $\gamma_c > \omega_M$ and $\epsilon \ll \omega_M$. This figure exhibits phonon sideband peaks, and hence indicates that $\omega_M > \epsilon$ also provides the condition for observing the phonon sideband peaks due to the second line in Eq. (19). We point out that this provides a way to characterize the coupling strength g from the scattering spectrum in the case of $\gamma_c > \omega_M$. Another benefit in the near-monochromatic case is that we can conveniently control the exciting transition by choosing the frequency of the incident photon. In Figs. 5(b,c), we choose the frequency of the incident photon as $\Delta_0 = \delta^{(1)}$ and $\Delta_0 = \delta^{(1)} + 2\omega_M^{(1)}$ to resonantly excite the system from $|0\rangle_a|0\rangle_b$ to $|1\rangle_a|\tilde{0}\rangle_b$ and $|1\rangle_a|\tilde{2}\rangle_b$, respectively. In the emission process, the membrane will experience the transitions from $|\tilde{0}\rangle_b$ and $|\tilde{2}\rangle_b$ to $|n\rangle_b$ ($n = 0, 2, 4, ...$). Therefore, the maximal frequency sideband peaks should be located at $\Delta_k = \delta^{(1)}$ and $\delta^{(1)} + 2\omega_M^{(1)}$, respectively. In addition, the period of these peaks is $2\omega_M$. Similar to the emission case, the scattering spectrum also depends on the initial state of the membrane. In Fig. 5(d), we plot the scattering spectrum when

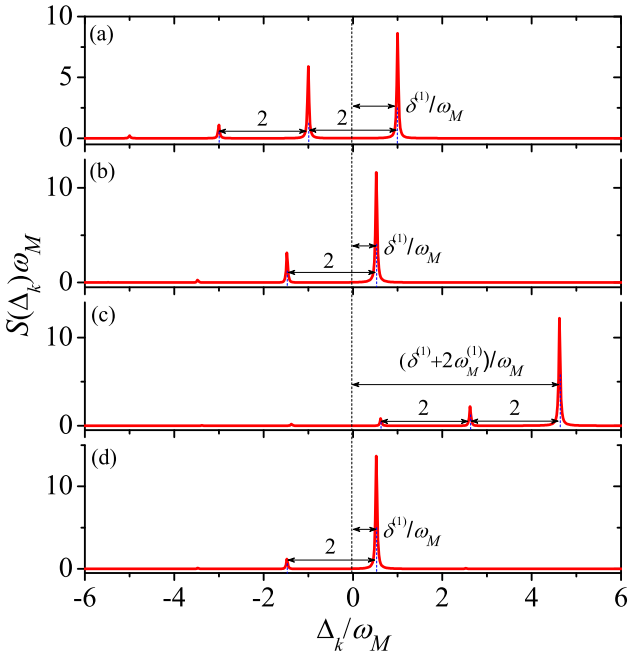

FIG. 5. (Color online) Scattering spectrum $S(\Delta_k)$ versus Δ_k. The panel (a) is plotted in the unresolved-sideband regime ($g/\omega_M = 2$ and $\gamma_c/\omega_M = 1.5$), while panels (b-d) are plotted in the resolved-sideband regime ($g/\omega_M = 0.8$ and $\gamma_c/\omega_M = 0.2$). The frequency center Δ_0 of the incident photon is $\delta^{(1)} + 2\omega_M^{(1)}$ in (c), and $\delta^{(1)}$ in other panels. The membrane's initial state is the ground state $|0\rangle_b$ in panels (a-c) and the coherent state $|\alpha = 1\rangle_b$ in (d). The parameter $\epsilon/\omega_M = 0.02$.

the membrane's initial state is coherent state $|\alpha = 1\rangle_b$. Though the initial coherent state contains both even- and odd-parity states, the spectrum only exhibits similar peaks as those in Fig. 5(b). This is because the incident photon (with $\Delta_0 = \delta^{(1)}$) only resonantly excites the mirror from $|0\rangle_b$ to $|\tilde{0}\rangle_b$; other transitions from $|n\rangle_b$ to $|\tilde{n}'\rangle_b$ ($n, n' = 1, 2, 3, ...$, with the same parity) are significantly suppressed due to the large detuning. A further photon emission process induces the transitions from $|\tilde{0}\rangle_b$ to $|n\rangle_b$ ($n = 0, 2, 4, ...$).

V. CONCLUSION AND REMARKS

In conclusion, we have analytically studied the single-photon emission and scattering in a quadratically-coupled optomechanical model. By treating the optomechanical cavity and its environment as a whole system, we have obtained the emission and scattering solutions using the Laplace-transform method. Based on our solutions, we have calculated the emission and scattering spectra, and indicated the connection between the spectral features and the system's inherent parameters. In particular, we have clarified the condition under which phonon sideband peaks can be observed in the photon spectra. In the resolved-sideband regime $\omega_M > \gamma_c$, the phonon sidebands are visible when $g > \gamma_c$, while the condition for resolving the photon-state frequency shift $\delta^{(1)}$ is $g > \gamma_c(1 + \gamma_c/\omega_M)$.

Finally, we give some remarks on the quadratic coupling strength. Though current quadratic couplings are too weak to reach the single-photon strong-coupling regime, recent advances have been made in the enhancement of this coupling strength. In quadratic optomechanics, the coupling strength is $g = \frac{1}{2}\omega_c''(0)x_{\rm zpf}^2$, where $x_{\rm zpf}$ is the zero-point fluctuation of the mechanical membrane, and $\omega_c''(0) = \frac{\partial^2\omega_c(x)}{\partial x^2}|_{x=0}$, with $\omega_c(x)$ being the x-dependent cavity frequency. Recently, the value of $\omega_c''(0)$ has been increased significantly from about 30 MHz/nm^2 [27] to 20 GHz/nm^2 [34] using a fiber cavity with a smaller mode size. For a $x_{\rm zpf} \sim 5$ pm, suggested in Ref. [22], the coupling strength g can reach several kHz. In addition, a recent proposal [41] estimated a quadratic coupling $g \sim 2\pi \times 0.7$ MHz in a near-field optomechanical system.

ACKNOWLEDGMENTS

JQL is supported by the Japan Society for the Promotion of Science (JSPS) Foreign Postdoctoral Fellowship No. P12503. FN is partially supported by the ARO, JSPS-RFBR contract No. 12-02-92100, Grant-in-Aid for Scientific Research (S), MEXT Kakenhi on Quantum Cybernetics, and the JSPS via its FIRST program.

[1] T. J. Kippenberg and K. J. Vahala, Science **321**, 1172 (2008).
[2] F. Marquardt and S. M. Girvin, Physics **2**, 40 (2009).
[3] M. Aspelmeyer, T. J. Kippenberg, and F. Marquardt, e-print arXiv:1303.0733.
[4] C. K. Law, Phys. Rev. A **51**, 2537 (1995).
[5] S. Mancini, V. I. Manko, and P. Tombesi, Phys. Rev. A **55**, 3042 (1997).
[6] S. Bose, K. Jacobs, and P. L. Knight, Phys. Rev. A **56**, 4175 (1997).
[7] W. Marshall, C. Simon, R. Penrose, and D. Bouwmeester, Phys. Rev. Lett. **91**, 130401 (2003).
[8] K. Stannigel, P. Komar, S.J.M. Habraken, S.D. Bennett, M.D. Lukin, P. Zoller, and P. Rabl, Phys. Rev. Lett. **109**, 013603 (2012).
[9] M. Ludwig, A. H. Safavi-Naeini, O. Painter, and F. Marquardt, Phys. Rev. Lett. **109**, 063601 (2012).
[10] S. Gupta, K. L. Moore, K. W. Murch, and D. M. Stamper-Kurn, Phys. Rev. Lett. **99**, 213601 (2007).
[11] F. Brennecke, S. Ritter, T. Donner, and T. Esslinger, Science **322**, 235 (2008).
[12] M. Eichenfield, J. Chan, R. M. Camacho, K. J. Vahala, and O. Painter, Nature (London) **462**, 78 (2009).
[13] P. Rabl, Phys. Rev. Lett. **107**, 063601 (2011).
[14] A. Nunnenkamp, K. Børkje, and S. M. Girvin, Phys. Rev. Lett. **107**, 063602 (2011).
[15] T. Hong, H. Yang, H. Miao, and Y. Chen, e-print

arXiv:1110.3348.
[16] J. Q. Liao, H. K. Cheung, and C. K. Law, Phys. Rev. A **85**, 025803 (2012).
[17] B. He, Phys. Rev. A **85**, 063820 (2012).
[18] X. W. Xu, Y. J. Li, and Y. X. Liu, Phys. Rev. A **87**, 025803 (2013).
[19] A. Kronwald, M. Ludwig, and F. Marquardt, Phys. Rev. A **87**, 013847 (2013).
[20] J. Q. Liao and C. K. Law, Phys. Rev. A **87**, 043809 (2013).
[21] X. Y. Lü, W. M. Zhang, S. Ashhab, Y. Wu, and F. Nori, e-print arXiv:1210.8299.
[22] J. D. Thompson, B. M. Zwickl, A. M. Jayich, F. Marquardt, S. M. Girvin, and J. G. E. Harris, Nature (London) **452**, 72 (2008).
[23] M. Bhattacharya, H. Uys, and P. Meystre, Phys. Rev. A **77**, 033819 (2008).
[24] M. Bhattacharya and P. Meystre, Phys. Rev. A **78**, 041801(R) (2008).
[25] A. Rai and G. S. Agarwal, Phys. Rev. A **78**, 013831 (2008).
[26] A. M. Jayich, J. C. Sankey, B. M. Zwickl, C. Yang, J. D. Thompson, S. M. Girvin, A. A. Clerk, F. Marquardt, and J. G. E. Harris, New J. Phys. **10**, 095008 (2008).
[27] J. C. Sankey, C. Yang, B. M. Zwickl, A. M. Jayich, and J. G. E. Harris, Nature Phys. **6**, 707 (2010).
[28] A. Nunnenkamp, K. Børkje, J. G. E. Harris, and S. M. Girvin, Phys. Rev. A **82**, 021806(R) (2010).
[29] T. P. Purdy, D. W. C. Brooks, T. Botter, N. Brahms, Z. Y. Ma, and D. M. Stamper-Kurn, Phys. Rev. Lett. **105**, 133602 (2010).
[30] S. Huang and G. S. Agarwal, Phys. Rev. A **83**, 023823 (2011).
[31] C. Biancofiore, M. Karuza, M. Galassi, R. Natali, P. Tombesi, G. Di Giuseppe, and D. Vitali, Phys. Rev. A **84**, 033814 (2011).
[32] H. K. Cheung and C. K. Law, Phys. Rev. A **84**, 023812 (2011).
[33] Z. J. Deng, Y. Li, M. Gao, and C. W. Wu, Phys. Rev. A **85**, 025804 (2012).
[34] N. E. Flowers-Jacobs, S. W. Hoch, J. C. Sankey, A. Kashkanova, A. M. Jayich, C. Deutsch, J. Reichel, and J. G. E. Harris, Appl. Phys. Lett. **101**, 221109 (2012).
[35] L. F. Buchmann, L. Zhang, A. Chiruvelli, and P. Meystre, Phys. Rev. Lett. **108**, 210403 (2012).
[36] A. Xuereb and M. Paternostro, Phys. Rev. A **87**, 023830 (2013).
[37] H. Shi and M. Bhattacharya, Phys. Rev. A **87**, 043829 (2013).
[38] H. T. Tan, F. Bariani, G. X. Li, and P. Meystre, e-print arXiv:1302.7087.
[39] X. G. Zhan, L. G. Si, A. S. Zheng, and X. X. Yang, J. Phys. B: At. Mol. Opt. Phys. **46**, 025501 (2013).
[40] Equation (11) shows that both $\omega_M^{(1)} > \gamma_c$ and $\omega_M > \gamma_c$ might be the resolved-sideband condition. For a positive g, then $\omega_M > \gamma_c$ could make sure that the two conditions are met, because of $\omega_M^{(1)} > \omega_M$. We found that, in the case of $\omega_M^{(1)} > \gamma_c > \omega_M$, the phonon-sideband evidence is negligible. So, in this paper, we consider $\omega_M > \gamma_c$ as the resolved-sideband condition.
[41] H. K. Li, Y. C. Liu, X. Yi, C. L. Zou, X. X. Ren, and Y. F. Xiao, Phys. Rev. A **85**, 053832 (2012).